Research Article

INTERNATIONAL JOURNAL OF ADVANCED ROBOTIC SYSTEMS

International Journal of Advanced Robotic Systems
May-June 2021: 1–15

DOI: 10.1177/17298814211011035
journals.sagepub.com/home/arx
SAGE

Extended state observer-based integral line-of-sight guidance law for path following of underactuated unmanned surface vehicles with uncertainties and ocean currents

Mingcong Li, Chen Guo and Haomiao Yu

Abstract

This article focuses on the problem of path following for underactuated unmanned surface vehicles (USVs) considering model uncertainties and time-varying ocean currents. An extended state observer (ESO)-based integral line-of-sight (ILOS) with an integral sliding mode adaptive fuzzy control scheme is proposed as the main control framework. First, a novel ESO is employed to estimate the surge and sway velocities based on the kinetic model, which are difficult to measure directly. Then, the adaptive ILOS guidance law is proposed, in which the integral vector is incorporated into the adaptive method to estimate the current velocities. Meanwhile, an improved fuzzy algorithm is introduced to optimize the look-ahead distance. Second, the controller is extended to deal with the USV yaw and surge velocity signal tracking using the integral sliding mode technique. The uncertainties of the USV are approximated via the adaptive fuzzy method, and an auxiliary dynamic system is presented to solve the problem of actuator saturation. Then, it is proved that all of the error signals in the closed-loop control system are uniformly ultimately bounded. Finally, a comparative simulation substantiates the availability and superiority of the proposed method for ESO-based ILOS path following of USV.

Keywords

Unmanned surface vehicles, ocean currents, line-of-sight, path following, actuator saturation

Date received: 19 March 2020; accepted: 31 March 2021

Topic Area: Robot Manipulation and Control
Topic Editor: Yangquan Chen
Associate Editor: Yangquan Chen

Introduction

In recent decades, intelligent control of unmanned surface vehicles (USVs) has become one of the most challenging topics in the nonlinear control community and has attracted great attention in the marine, military, and commerce fields for applications, such as path following, collision avoidance, and formation control.[1–5] The problem of USV path following has expanded over the past decade and is a thorny aspect of USV intelligent control because of its complicated mathematical model. Additionally, a difficult problem is that only the surge and yaw direction can be directly controlled, while the sway velocity is passive for most USVs.

Most USVs are underactuated in that the number of actuators in the mechanism is less than its degree of

College of Marine Electrical Engineering, Dalian Maritime University, Dalian, China

Corresponding author:
Chen Guo, College of Marine Electrical Engineering, Dalian Maritime University, Dalian 116026, China.
Email: dmuguoc@126.com

freedom. Although an underactuated system is more complex than a full-drive system, the former possesses several advantages including conservation of energy, material, and space.[6,7] The authors proposed the underactuated spherical parallel mechanism-based robotic ankle exoskeleton, and the lightweight mechanism in low-carbon design was verified. In the literature,[8] a detailed calculation model for each stage of the sustainable supply chain was proposed, and findings revealed that the underactuated system can be used to achieve lightweight and energy saving, thereby leading to a low carbon footprint. The underactuated system has its special values, but it needs to achieve breakthroughs or unprecedented innovations in both theoretical and practical techniques. At present, research on this type of system has become popular in USVs and robotics,[6–10] and the control of underactuated systems has been researched mainly by state stabilization, trajectory tracking, and path following.[6] High nonlinearity renders the control of such tasks particularly challenging.

The control objective of the USV path following is to keep it following a reference path without time constraints. In other words, the position tracking errors should be ultimately bounded. A conventional method to achieve convergence to the reference path is to apply a line-of-sight (LOS) guidance law emulating an experienced mariner,[11] this method has been popularized in the USV path following system.[1,12,13] Several authors have studied the traditional LOS guidance law, but it is vulnerable to external influencing factors, such as wind, waves, and ocean currents. The most severe problem is that the sideslip angle of the USV magnifies the tracking error signals and can even lead to divergence or oscillation of the entire cascade control system. The most straightforward method to compensate for the sideslip angle is to measure it using high-precision sensors.[14] However, these sensors are difficult to implement due to their high costs in practice. Some researchers solve these problems by coalescing the sideslip angle with the course angle. One such scheme is the integral LOS (ILOS) method,[13] which was devised by adding an integral term to the original LOS guidance law. Similarly, Mu et al.[15] developed an adaptive LOS (ALOS) scheme, in which an adaptive method was introduced to calculate the sideslip angle. The ALOS scheme is a specific type of ILOS with a time-invariant or slow time-varying sideslip angle. These methods seem incapable of dealing with a fast time-varying sideslip angle. Based on the above analysis, extended state observer (ESO)-based LOS (ELOS)[16] and predictor-based LOS (PLOS)[12] methods were proposed, in which the ESO and predictor were introduced to calculate the sideslip angles with any rate of change and encapsulated into the LOS guidance laws. However, the simplified operations in ELOS and PLOS require that the sideslip angle should be in a small range. In this context, Wang et al.[17] proposed a novel observer to precisely calculate the sideslip angle with any magnitudes within a short time. USVs have long suffered from ocean currents in practice, whereas the aforementioned studies did not consider ocean current velocities. Note that the ocean currents can destabilize the cascade system. Miao et al.[18] proposed a novel compound line-of-sight (CLOS) scheme, in which the sideslip angle and the time-varying ocean currents can be accurately estimated and compensated simultaneously. Given the accompanying computational complexity, an adaptive ILOS guidance law was presented by Zheng and Sun[19] and suited to any parametric path. Ocean currents could also be calculated based on the adaptive law.

The problem of control design in the execution module represents another indispensable aspect of the path-following cascade control system. Essentially, the execution module control system should be designed to force the USV state to track the reference signals of the proposed LOS guidance law. When controlling an underactuated system, the first problem is controllability; this system is complex and nonlinear, such that linear control theories cannot be directly applied. Underactuated systems must be analyzed using nonlinear controllability theory based on their own characteristics. Extensive research has presented controllability analysis of underactuated systems. From the mathematical standpoint, the authors[20–22] provided a theoretical basis for the controllability analysis in underactuated systems. The control of the underactuated system is always realized using motion coupling or dynamic coupling.[23–26] In a controllable system, an effective control technique is backstepping control, which has been widely adopted given its systematic calculated amount.[17,26,27] The backstepping technique can eliminate the constraint that the relative degree must be 1 in classical passive systems. However, the heavy calculation burden of backstepping makes some control strategies impractical. From this point of view, the active-disturbance-rejection controller (ADRC), trajectory linearization controller (TLC), and sliding mode controller (SMC) have been proposed by many researchers. In the literature,[28] a control scheme combining the LOS guidance law with the ADRC technique was proposed to make the USV follow a reference parameterized curved path. Liu et al.[29] introduced the TLC scheme in relation to USV path following and illuminated a new direction in TLC technology. Considering the robustness to external disturbances, parameter perturbations, and unmodeled dynamics, SMC is an effective and powerful advanced controllers that have been developed considerably in USV and robot areas.[30–35] In practical applications, SMC has successfully applied to underactuated biped robot,[36] satellites,[37] and overhead crane.[38] For example, sliding mode observer was designed by Van et al.[39] to estimate the robot velocities in the presence of model uncertainties and external disturbances. A backstepping sliding mode AUV path-following control algorithm was proposed by Liang et al.[40] However, the single SMC usually cannot satisfy the system requirement, such as high efficiency and strong robustness. In this case, a hybrid

control scheme that switched between proportional-derivative (PD) control and SMC was proposed by Ouyang et al.[31] for tracking control of robot manipulators, where PD control was used to stabilize the controlled system, while SMC was used to compensate the disturbance and uncertainty and reduce tracking errors. In the literature,[30] the integral SMC (ISMC) was first employed for USV trajectory tracking. Moreover, the ISMC was introduced to the USV path following control[26] and applied in the attitude loop and surge velocity loop, respectively, findings were fairly encouraging. In the literature,[41] an adaptive SMC (ASMC) method was designed for the parallel robot with six prismatic actuators in the presence of actuator fault. In the literature,[42] a proportional-integral-derivative SMC (PID-SMC) trajectory tracking scheme was proposed, in which the PID-SMC can ensure all the tracking errors converge to zero within a finite time in sliding and approaching mode. Besides, terminal SMC (TSMC)[43] and iterative SMC[44] were also widely used in USV and robot motion control. Considering the chattering caused by the sign functions in SMC, most actuators cannot suffer from this phenomenon in reality. Researchers have thus presented many approaches to preventing this issue, such as by using the continuous sigmoid function instead of the sign function,[45] adding a filter,[46] introducing a fuzzy/neural network to approximate the sign function,[47] or applying mathematical optimization to the switching function.[48]

System uncertainty and disturbance are common in practical control systems. The robustness against them is critical for motion control of USV. A variety of methods were proposed to deal with the uncertainty, ranging from Fourier series expansion,[49] observers,[50] and neural networks[51–53] to fuzzy techniques. Fuzzy control is an early form of intelligent control and it imitates the ambiguity of human's thought and controls objects using the control experience of human experts.[6] A weakness of fuzzy techniques is that approximator accuracy relies on the number of nodes. An effective approach involves estimating the norm of the ideal weighting vector by replacing the vector elements. From this point of view, in the literature,[34] an adaptive fuzzy control method was proposed to estimate model uncertainty and achieve remarkable tracking performance in terms of both tracking and unknown estimation. In the literature,[54] the fuzzy techniques were used to estimate the model uncertainty and external disturbance simultaneously. Considering the structure of approximator, Wang and Er[55] proposed a self-constructing fuzzy control USV trajectory tracking scheme, which contained self-learning membership functions and parameter adaptation.

Every input into real systems should be bounded by actuators' physical restrictions. The actuator saturation (i.e. input saturation) tends to be ignored when designing control systems. Actuator saturation can strongly influence the stability of systems, such as undershooting, lag, and performance degradation. To solve this physical problem, Chen et al.[56] proposed an auxiliary dynamic system to compensate for the input constraints. The system states were applied for the adaptive tracking control design in uncertain MIMO nonlinear systems. In the literature,[57] a finite-time trajectory tracking scheme was proposed based on PD plus dynamics compensation in the presence of input saturation, where the Sat function was introduced to deal with the saturation problem. In the literature,[19] an auxiliary design system was presented to compensate for the surge and yaw controller in an underactuated USV, and the uniformly ultimately bounded (UUB) stability was confirmed for the cascade path following system.

In this article, an ESO-based ILOS (EILOS) guidance law and adaptive fuzzy SMC (EIAFSM) with actuator saturation are proposed for USV path following in the presence of ocean current velocities and external model uncertainties. The ESO is developed to identify surge and sway velocities considering their immeasurability, and the ILOS guidance law is designed to produce the reference heading angle. In addition, an improved algorithm is proposed for look-ahead distance. Then, the SMC is designed to maintain the USV surge velocity and heading angle tracking the reference signals generated by the LOS guidance law. Meanwhile, the USV model uncertainty and sign functions in the control law are estimated using the fuzzy logic system (FLS), and an auxiliary system is provided to compensate for the part exceeding the actuator limit.

The remainder of this article is structured as follows. Several necessary preliminaries and explanations about the USV model are detailed in the second section. The EILOS guidance scheme is introduced in the third section. The fourth section outlines the actuator control method for USVs. The system convergence analysis is presented in the fifth section. The sixth section provides an example to illustrate the feasibility of the proposed method, and the seventh section offers our conclusion and directions for future work.

Preliminaries

Lemmas

Definition 1. $\mathbb{R}^n$ is the n-dimensional Euclidean space. The solution of the differential equation is x and $x(t_0) = x_0$.[58] For a set containing the origin $W \subset \mathbb{R}^n$, the system is UUB if there is a non-negative constant $T(x_0, W) < \infty$, so that the following equation holds for all $t \geq t_0 + T$

$$\| x(t_0) \| < \delta \Rightarrow x(t) \in W \tag{1}$$

Lemma 1. If $x = 0$ is an equilibrium point of the system $\dot{x} = f(x,t)$, and the function f is Lipschitz, there exists a positive Lyapunov function V satisfying[58,59]

$$\dot{V} = \frac{\partial V}{\partial x} f(x,t) \leq -CV + \rho \leq 0, \forall t \geq 0, \forall x \in \mathbb{R}^n \tag{2}$$

where C is a non-negative parameter and $\rho < \infty$. The system $\dot{x} = f(x,t)$ is UUB.

Lemma 2. The USV input signal τ_i is limited by $-\tau_{i\max}$ and $\tau_{i\max}$, such that $-\tau_{i\max} \le \tau_i \le \tau_{i\max}$.[19] The relational expression between the real τ_i and the command τ_{i0} is

$$\tau_i = \begin{cases} \tau_{i\max}, \tau_{i0} > \tau_{i\max} \\ \tau_{i0}, -\tau_{i\max} \le \tau_{i0} \le \tau_{i\max} \\ -\tau_{i\max}, \tau_{i0} < -\tau_{i\max} \end{cases} \tag{3}$$

Lemma 3. For $a, b \ge 0$, the Young's inequality holds[60]

$$ab \le \frac{\delta^m}{m}|a|^m + \frac{1}{n\delta^n}|b|^n \tag{4}$$

where δ is positive, $m, n > 1$ and $(m-1)(n-1) = 1$. When $m = n = 2, \delta = 1$, inequality (4) becomes $ab \le \frac{1}{2}a^2 + \frac{1}{2}b^2$. In this case, the right side of the inequality sign is non-negative. Thus, if $a \le 0$ or $b \le 0$, the inequality also holds.

Unmanned surface vehicle models

This subsection describes the USVs' kinematic and dynamic models with ocean currents. The mathematical model of a USV on a horizontal plane can be described as follows

$$\begin{cases} \dot{x} = u_r\cos\psi - v_r\sin\psi + V_x \\ \dot{y} = u_r\sin\psi + v_r\cos\psi + V_y \\ \dot{\psi} = r \\ \dot{u}_r = \boldsymbol{H}_u(v_r, r) - \dfrac{d_{11}}{m_{11}}u_r + \tau_u + \delta_u \\ \dot{v}_r = \boldsymbol{E}(u_r)r + \boldsymbol{F}(u_r)v_r + \delta_v \\ \dot{r} = \boldsymbol{H}_r(u_r, v_r, r) + \tau_r + \delta_r \end{cases} \tag{5}$$

where (x, y) provide the positional information and ψ denotes the heading angle. (u_r, v_r, r) represent the USV relative surge velocity, the sway velocity, and the yaw rate within the body-fixed frame, respectively. (V_x, V_y) describe the x, y directions of ocean current velocities within the inertial frame. Define $\boldsymbol{R}(\psi) = \begin{bmatrix} \cos\psi & -\sin\psi \\ \sin\psi & \cos\psi \end{bmatrix}$ and $[u_c, v_c]^T = \boldsymbol{R}(\psi)[V_x, V_y]^T$, where (u_c, v_c) describe the velocities of ocean current within the body-fixed frame. $[u, v]^T = [u_r, v_r]^T + [u_c, v_c]^T$, where (u, v) are the absolute USV velocities. (τ_u, τ_r) represent the input signals that directly control the actuator. The external disturbances can be expressed as $(\delta_u, \delta_v, \delta_r)$. The definitions of $\boldsymbol{H}_u(v_r, r)$, $\boldsymbol{E}(u_r)$, $\boldsymbol{F}(u_r)$, and $\boldsymbol{H}_r(u_r, v_r, r)$ are given in Appendix.

Assumption 1. The absolute USV resultant velocity U, heading angle ψ, and yaw rate r are measurable, but the relative velocities u_r and v_r are not.

Assumption 2. δ_u, δ_v, and δ_r are bounded, their upper bounds can be described as (η_1, η_2, η_3), which are unknown.

Assumption 3. The ocean currents are assumed to be slow changing such that $\dot{V}_x \approx \dot{V}_y \approx 0$ and bounded by $V_{\max}$. The magnitudes of ocean currents are much lower than the USV velocities.

Assumption 4. The time derivatives of u_r and v_r are bounded.

Remark 1. In Assumption 1, we can easily determine the state vectors U,ψ, and r from common navigational instruments. The relative velocities are difficult to measure with common apparatuses.[61] Assumptions 2 and 3 are reasonable due to the finite energy of external disturbances including ocean currents,[62] and similar assumptions appear in the literature.[18] For Assumption 4, similar theories can be found in Proposition 1[63] and Assumption 1.[16] This assumption is justified given that the energy of the USV actuator is finite and abrupt signal change is not allowed, thereby leading to $|\dot{u}(\dot{v})_r| \le \omega_{\max}$, where $\omega_{\max}$ is a positive constant.

Control objective

This article aims to propose a control algorithm to keep the USV following a prescribed path parameterized by $(x_k(\varsigma), y_k(\varsigma))$, such that the velocities and position tracking errors of USV converge to a small range ultimately, that is, $\lim_{t\to\infty}(x - x_k) \le \ell_x$, $\lim_{t\to\infty}(y - y_k) \le \ell_y$, and $\lim_{t\to\infty}(u_r - u_{rd}) \le \ell_u$, where u_{rd} denotes the desired relative surge velocity and ℓ_x, ℓ_y, ℓ_u are bounded constants.

Remark 2. More precisely, the objective of the velocity is to realize $\lim_{t\to\infty} U \to U_d$, where U_d represents the desired absolute resultant velocity. If V_x, V_y, u_r and v_r are known or accurately estimated, then, we can easily calculate the desired relative sway velocity u_{rd}. Therefore, it is reasonable for u_{rd} to be the velocity objective.

Guidance subsystem design

The schematic diagram of USV path following and an EILOS guidance law are presented in this section. The LOS geometry is shown in Figure 1.

Let ς describe the desired path $(x_k(\varsigma), y_k(\varsigma))$ and the tangential angle of the path is defined as $\gamma_k(\varsigma) = a\tan2(y'_k(\varsigma), x'_k(\varsigma))$, satisfying $\gamma_k(\varsigma) := [-\pi, \pi]$, where y'_k and x'_k denote the partial derivatives of y_k and x_k, respectively. The sideslip angle that is always ignored by some researchers can be expressed as $\beta = a\tan2(v, u)$. Note that the USV velocities in system (5) are relative due to the ocean currents. To facilitate calculations, define $\beta_r = a\tan2(v_r, u_r)$ as the relative sideslip angle that can only be a dummy variable.

Assumption 5. The guidance signal ψ_d can be completely tracked by the actual heading angle in the guidance part regardless of the control effects of τ_u and τ_r, that is, $\psi = \psi_d$.

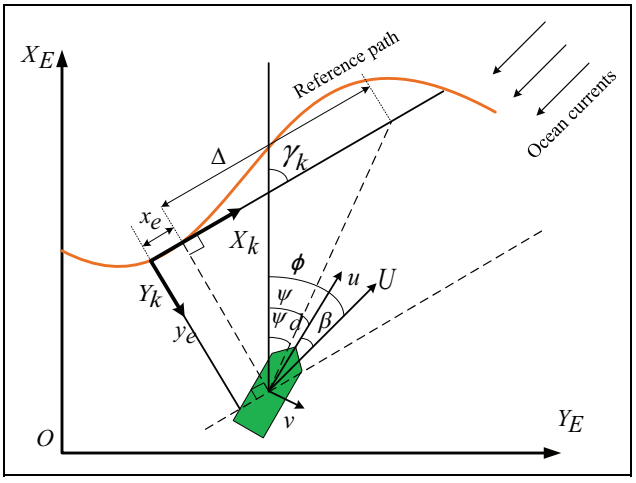

Figure 1. LOS guidance geometry. LOS: line-of-sight.

As shown in Figure 1, the along- and cross-tracking errors (x_e, y_e) of USV can be expressed as

$$\begin{bmatrix} x_e \\ y_e \end{bmatrix} = \begin{bmatrix} \cos\gamma_k & -\sin\gamma_k \\ \sin\gamma_k & \cos\gamma_k \end{bmatrix}^T \begin{bmatrix} x - x_k(\varsigma) \\ y - y_k(\varsigma) \end{bmatrix} \tag{6}$$

Similar to equation (6), we have

$$\begin{bmatrix} \dot{x}_k(\varsigma) \\ \dot{y}_k(\varsigma) \end{bmatrix} = \begin{bmatrix} \cos\gamma_k & -\sin\gamma_k \\ \sin\gamma_k & \cos\gamma_k \end{bmatrix} \begin{bmatrix} u_m \\ 0 \end{bmatrix} \tag{7}$$

where u_m represents the virtual speed of the desired path and $u_m = \dot{\varsigma}\sqrt{x'^2_k + y'^2_k}$.

The time derivative of the along-tracking error is expressed by

$$\begin{aligned} \dot{x}_e &= \dot{x}\cos\gamma_k + \dot{y}\sin\gamma_k - \dot{x}_k(\varsigma)\cos\gamma_k - \dot{y}_k(\varsigma)\sin\gamma_k \\ &\quad + \dot{\gamma}_k \underbrace{[-(x - x_k(\varsigma))\sin\gamma_k + (y - y_k(\varsigma))\cos\gamma_k]}_{y_e} \end{aligned} \tag{8}$$

Similarly, we have

$$\begin{aligned} \dot{y}_e &= -\dot{x}\sin\gamma_k + \dot{y}\cos\gamma_k + \dot{x}_k(\varsigma)\sin\gamma_k - \dot{y}_k(\varsigma)\cos\gamma_k \\ &\quad - \dot{\gamma}_k \underbrace{[(x - x_k(\varsigma))\cos\gamma_k + (y - y_k(\varsigma))\sin\gamma_k]}_{x_e} \end{aligned} \tag{9}$$

Substituting equations (5) to (7) into equations (8) and (9) results in

$$\begin{cases} \dot{x}_e = u_r\cos(\psi_d - \gamma_k) - v_r\sin(\psi_d - \gamma_k) + y_e\dot{\gamma}_k - u_m \\ \qquad +\theta_x \\ \dot{y}_e = u_r\sin(\psi_d - \gamma_k) + v_r\cos(\psi_d - \gamma_k) - x_e\dot{\gamma}_k + \theta_y \end{cases} \tag{10}$$

where $\theta_x = V_c\cos(\beta_c - \gamma_k)$ and $\theta_y = V_c\sin(\beta_c - \gamma_k)$, in which $V_c = \sqrt{V_x^2 + V_y^2}$ and $\beta_c = a\tan2(V_y, V_x)$. θ_x and θ_y are bounded under Assumption 3.

To estimate the relative velocities of the USV, two novel ESOs are proposed as follows

$$\begin{cases} \hat{u}_r = p_1 + k_1 x_e \\ \dot{p}_1 = -k_1(\hat{u}_r\cos(\psi_d - \gamma_k) - \hat{v}_r\sin(\psi_d - \gamma_k) + \dot{\gamma}_k y_e \\ \qquad -u_m) + y_e\sin(\psi_d - \gamma_k) + x_e\cos(\psi_d - \gamma_k) \end{cases} \tag{11}$$

and

$$\begin{cases} \hat{v}_r = p_2 + k_1 y_e \\ \dot{p}_2 = -k_1(\hat{u}_r\sin(\psi_d - \gamma_k) + \hat{v}\cos(\psi_d - \gamma_k) + \dot{\gamma}_k x_e) \\ \qquad +y_e\cos(\psi_d - \gamma_k) - x_e\sin(\psi_d - \gamma_k) \end{cases} \tag{12}$$

where $\hat{u}_r$ and $\hat{v}_r$ are the estimations of u_r and v_r, respectively, and k_1 is a positive parameter. Define the estimation errors $\tilde{u}_r = \hat{u}_r - u_r$ and $\tilde{v}_r = \hat{v}_r - v_r$. By combining equations (10) to (12), the corresponding error dynamics of the velocity estimations can be written as

$$\begin{cases} \dot{\tilde{u}}_r = \dot{\hat{u}}_r - \dot{u}_r = \dot{p}_1 + k_1\dot{x}_e - \dot{u}_r \\ \quad = -k_1\tilde{u}_r\cos(\psi_d - \gamma_k) + k_1\tilde{v}_r\sin(\psi_d - \gamma_k) + k_1\theta_x \\ \quad +y_e\sin(\psi_d - \gamma_k) + x_e\cos(\psi_d - \gamma_k) - \dot{u}_r \\ \dot{\tilde{v}}_r = \dot{\hat{v}}_r - \dot{v}_r = \dot{p}_2 + k_1\dot{y}_e - \dot{v}_r \\ \quad = -k_1\tilde{v}_r\cos(\psi_d - \gamma_k) - k_1\tilde{u}_r\sin(\psi_d - \gamma_k) + k_1\theta_y \\ \quad +y_e\cos(\psi_d - \gamma_k) - x_e\sin(\psi_d - \gamma_k) - \dot{v}_r \end{cases} \tag{13}$$

Remark 3. The ESO system is significantly different from the ESOs provided in the literature.[63] We take ocean currents into account, two compulsory terms θ_x and θ_y are added into the error system (13). In addition, to achieve the stability of a more complicated guidance system, there are two additional terms $y_e\cos(\psi_d - \gamma_k)$ and $x_e\sin(\psi_d - \gamma_k)$ of the ESO system.

Note that $u_r = \hat{u}_r - \tilde{u}_r$ and $v_r = \hat{v}_r - \tilde{v}_r$, rewrite equation (10) as

$$\begin{cases} \dot{x}_e = \hat{u}_r\cos(\psi_d - \gamma_k) - \tilde{u}_r\cos(\psi_d - \gamma_k) - \hat{v}_r\sin(\psi_d - \gamma_k) \\ \qquad +\tilde{v}_r\sin(\psi_d - \gamma_k) + y_e\dot{\gamma}_k - u_m + \theta_x \\ \dot{y}_e = \hat{u}_r\sin(\psi_d - \gamma_k) - \tilde{u}_r\sin(\psi_d - \gamma_k) + \hat{v}_r\cos(\psi_d - \gamma_k) \\ \qquad -\tilde{v}_r\cos(\psi_d - \gamma_k) - x_e\dot{\gamma}_k + \theta_y \end{cases} \tag{14}$$

The guidance law is presented as

$$\psi_d = \gamma_k - \hat{\beta}_r + \arctan\left(\frac{-y_e - \alpha_r}{\Delta}\right) \tag{15}$$

where $\hat{\beta}_r = a\tan2(\hat{v}_r, \hat{u}_r)$, $\Delta > 0$ represents the look-ahead distance, and the integral term α_r is the virtual input that is used to shape the dynamics of the system.

Define $(\hat{\theta}_x, \hat{\theta}_y)$ is the estimation of (θ_x, θ_y), $(\tilde{\theta}_x, \tilde{\theta}_y)$ are the estimation errors, and $\tilde{\theta}_x = \theta_x - \hat{\theta}_x$, $\tilde{\theta}_y = \theta_y - \hat{\theta}_y$.

In equation (14), u_m can be treated as the moving speed of the reference path and is proposed as

$$u_m = \hat{u}_r\cos(\psi_d - \gamma_k) - \hat{v}_r\sin(\psi_d - \gamma_k) + k_2 x_e + \hat{\theta}_x \quad (16)$$

where k_2 is a positive constant. Therefore, the update law of the path variable ς can be expressed as

$$\dot{\varsigma} = \frac{\hat{u}_r\cos(\psi_d - \gamma_k) - \hat{v}_r\sin(\psi_d - \gamma_k) + k_2 x_e + \hat{\theta}_x}{\sqrt{x_k'^2 + y_k'^2}} \quad (17)$$

Remark 4. Note that the physical meaning of virtual variable u_m is that the speed of the reference path and its value depend on some USV state variables, such as u_r, v_r, x_e, and ψ_d. One can adjust the tracking speed between the real and reference path, that is, the desired path also tracks the real path to some extent, dramatically reducing the computational burden.

The derivative of y_e can be rewritten as

$$\begin{aligned}\dot{y}_e = \; & \hat{U}_r\sin(\psi_d + \hat{\beta}_r - \gamma_k) - \tilde{u}_r\sin(\psi_d - \gamma_k) \\ & -\tilde{v}_r\cos(\psi_d - \gamma_k) - x_e\dot{\gamma}_k + \theta_y\end{aligned} \quad (18)$$

where $\hat{U}_r$ is the estimate of relative resultant velocity and $\hat{U}_r = \sqrt{\hat{u}_r^2 + \hat{v}_r^2}$.

Substituting equation (15) into equation (18) yields

$$\begin{aligned}\dot{y}_e = \; & -\hat{U}_r\frac{y_e + \alpha_r}{\sqrt{(y_e + \alpha_r)^2 + \Delta^2}} - \tilde{u}_r\sin(\psi_d - \gamma_k) \\ & -\tilde{v}_r\cos(\psi_d - \gamma_k) - x_e\dot{\gamma}_k + \theta_y\end{aligned} \quad (19)$$

Note that the ocean current parameter θ_y can be eliminated by designing the virtual control input α_r in asymptotically as follows[64]

$$\frac{\hat{U}_r\alpha_r}{\sqrt{(y_e + \alpha_r)^2 + \Delta^2}} = \hat{\theta}_y \quad (20)$$

Then, the position errors dynamic system (14) becomes

$$\begin{cases}\dot{x}_e = -\tilde{u}_r\cos(\psi_d - \gamma_k) + \tilde{v}_r\sin(\psi_d - \gamma_k) + y_e\dot{\gamma}_k + \tilde{\theta}_x \\ \dot{y}_e = \; -\hat{U}_r\dfrac{y_e}{\sqrt{(y_e + \alpha_r)^2 + \Delta^2}} - \tilde{u}_r\sin(\psi_d - \gamma_k) \\ \qquad\quad -\tilde{v}_r\cos(\psi_d - \gamma_k) - x_e\dot{\gamma}_k + \tilde{\theta}_y\end{cases} \quad (21)$$

Solving for α_r given one feasible solution (the positive root) given by

$$\alpha_r = \frac{y_e\left(\frac{\hat{\theta}_y}{\hat{U}_r}\right)^2 - \frac{\hat{\theta}_y}{\hat{U}_r}\sqrt{\Delta^2\left(1 - \left(\frac{\hat{\theta}_y}{\hat{U}_r}\right)^2\right) + y_e^2}}{1 - \left(\frac{\hat{\theta}_y}{\hat{U}_r}\right)^2} \quad (22)$$

The condition $\left|\frac{\hat{\theta}_y}{\hat{U}_r}\right| < 1$ must be satisfied to guarantee that α_r is bounded.

Design the adaptive law for ocean currents parameters as follows

$$\begin{cases}\dot{\hat{\theta}}_x = \dfrac{1}{\Gamma_1}(x_e - \vartheta_1\hat{\theta}_x) \\ \dot{\hat{\theta}}_y = \dfrac{1}{\Gamma_2}(y_e - \vartheta_2\hat{\theta}_y)\end{cases} \quad (23)$$

Remark 5. The magnitudes of the ocean current velocities can be a far cry from USV. Therefore, if the initial conditions of $(\hat{\theta}_y, \hat{u}_r, \hat{v}_r)$ and the control parameters of the ESO and the adaptive law for ocean currents are set appropriately, $\left|\frac{\hat{\theta}_y}{\hat{U}_r}\right| < 1$ can be easily enforced.

Theorem 1. The subsystems (10) and (13), viewed as a guidance system containing position tracking errors (x_e, y_e) and estimation errors of the USV and ocean current velocities $(\tilde{u}_r, \tilde{v}_r, \tilde{\theta}_x, \tilde{\theta}_y)$, are UUB under Assumptions 3 to 5.

Proof. Considering the following Lyapunov function candidate (LFC) $V_1 = \frac{1}{2}x_e^2 + \frac{1}{2}y_e^2 + \frac{1}{2}\tilde{u}_r^2 + \frac{1}{2}\tilde{v}_r^2 + \frac{1}{2\Gamma_1}\tilde{\theta}_x^2 + \frac{1}{2\Gamma_2}\tilde{\theta}_y^2$. Taking the derivative of V_1 with respect to time, we obtain

$$\begin{aligned}\dot{V}_1 \; & = x_e\dot{x}_e + y_e\dot{y}_e + \tilde{u}_r\dot{\tilde{u}}_r + \tilde{v}_r\dot{\tilde{v}}_r + \frac{1}{\Gamma_1}\tilde{\theta}_x\dot{\tilde{\theta}}_x + \frac{1}{\Gamma_2}\tilde{\theta}_y\dot{\tilde{\theta}}_y \\ & = -k_2x_e^2 - \phi_1 y_e^2 - k_1\tilde{u}_r^2\cos(\psi_d - \gamma_k) - \dot{u}_r\tilde{u}_r - \dot{v}_r\tilde{v}_r \\ & \quad -k_1\tilde{v}_r^2\cos(\psi_d - \gamma_k) + x_e\tilde{\theta}_x + y_e\tilde{\theta}_y + k_1\tilde{u}_r\theta_x \\ & \quad +k_1\tilde{v}_r\theta_y - x_e\tilde{\theta}_x + \vartheta_1\tilde{\theta}_x\hat{\theta}_x - y_e\tilde{\theta}_y + \vartheta_2\tilde{\theta}_y\hat{\theta}_y\end{aligned} \quad (24)$$

where $\phi_1 = \frac{\hat{U}_r}{\sqrt{(y_e + \alpha_r)^2 + \Delta^2}} > 0$. According to Lemma 3, we can obtain

$$\begin{cases}\dot{u}_r\tilde{u}_r \le \dfrac{1}{2}\dot{u}_r^2 + \dfrac{1}{2}\tilde{u}_r^2 \\ \dot{v}_r\tilde{u}_r \le \dfrac{1}{2}\dot{v}_r^2 + \dfrac{1}{2}\tilde{v}_r^2 \\ k_1\tilde{u}_r\theta_x \le \dfrac{1}{2}\tilde{u}_r^2 + \dfrac{1}{2}k_1^2\theta_{x\max}^2 \\ k_1\tilde{v}_r\theta_y \le \dfrac{1}{2}\tilde{v}_r^2 + \dfrac{1}{2}k_1^2\theta_{y\max}^2 \\ \vartheta_1\tilde{\theta}_x\hat{\theta}_x = \vartheta_1\tilde{\theta}_x(\theta_x - \tilde{\theta}_x) \le \dfrac{\vartheta_1}{2}\theta_{x\max}^2 - \dfrac{\vartheta_1}{2}\tilde{\theta}_x^2 \\ \vartheta_2\tilde{\theta}_y\hat{\theta}_y = \vartheta_2\tilde{\theta}_y(\theta_y - \tilde{\theta}_y) \le \dfrac{\vartheta_1}{2}\theta_{y\max}^2 - \dfrac{\vartheta_1}{2}\tilde{\theta}_y^2\end{cases} \quad (25)$$

It yields that

$$\begin{aligned}\dot{V}_1 \leq\ & -(k_2-1)x_e^2-\phi_1 y_e^2-(k_1\cos(\psi_d-\gamma_k)-1)\tilde{u}_r^2 \\ & -(k_1\cos(\psi_d-\gamma_k)-1)\tilde{v}_r^2-\left(\frac{\vartheta_1}{2}-\frac{k_1}{2}\right)\tilde{\theta}_x^2 \\ & -\left(\frac{\vartheta_2}{2}-\frac{k_1}{2}\right)\tilde{\theta}_y^2+\frac{1}{2}\dot{u}_r^2+\frac{1}{2}\dot{v}_r^2 \\ & +\frac{\vartheta_1+k_1^2}{2}\theta_{x\max}^2+\frac{\vartheta_2+k_1^2}{2}\theta_{y\max}^2 \\ & \leq -2\mu_1 V_1+C_1\end{aligned} \tag{26}$$

where $\mu_1=\min\{k_2-1,\phi_{1\min},k_1\cos(\psi_d-\gamma_k)-1,(\vartheta_1-k_1)\Gamma_1/2,(\vartheta_2-k_1)\Gamma_2/2\}$ and $C_1=(\vartheta_1+k_1^2)\theta_{x\max}^2/2+(\vartheta_2+k_1^2)\theta_{y\max}^2/2+\dot{u}_r^2/2+\dot{v}_r^2/2$.

Thus, V_1 is a monotone decreasing function outside the range $\varpi_1=\{V_1\leq\frac{C_1}{2\mu_1}\}$ if $k_2-1>0, k_1\cos(\psi_d-\gamma_k)-1>0$ and gives

$$V_1\leq(V_1(0)-\frac{C_1}{2\mu_1})e^{-2\mu_1 t}+\frac{C_1}{2\mu_1} \tag{27}$$

and it follows that the errors $\tilde{u}_r$, $\tilde{v}_r$, x_e, y_e, $\tilde{\theta}_x$, and $\tilde{\theta}_y$ are UUB from Lemma 1.

The look-ahead distance, Δ, which impacts the tracking performance in the guidance system, has been deemed time invariant by most researchers.[1,12,17,26] This phenomenon leads to slow convergence of position-tracking errors. Actually, if the distance between the USV and the reference path is long, we should choose a smaller value for Δ to make the absolute value of y_e decrease more quickly; conversely, a larger Δ is corresponding to the close range between USV and reference path. In this context, Mu et al.[15] proposed a fuzzy algorithm of Δ according to this principle but did not consider the changing trend of y_e. Therefore, an improved FLS with the inputs being y_e and $\dot{y}_e$, the output being λ is introduced to optimize the value of Δ, where λ represents the gain. Then, the look-ahead distance Δ can be expressed as $\Delta=\Delta_{\min}+\lambda(\Delta_{\max}-\Delta_{\min})$. y_e, $\dot{y}_e$, and λ are equally divided into five parts. The fuzzy rules are given in Table 1, and the fuzzy surface of y_e, $\dot{y}_e$, and λ is shown in Figure 2.

As shown in Figure 3, the EILOS guidance law is a part of the whole path following the scheme of USV. We can employ the guidance law together with the actuator control system, which will be designed later using the sliding mode technique, FLS, and an auxiliary dynamic system.

Control subsystem design

In this section, the control laws τ_u and τ_r to achieve the desired velocity and heading angle are calculated.

Table 1. Fuzzy rules of Δ.

	$\dot{y}_e$				
y_e	NB	NS	Z	PS	PB
NB	VS	VS	VS	VS	S
NS	S	S	M	B	B
Z	B	VB	VB	VB	B
PS	B	B	M	S	S
PB	S	VS	VS	VS	VS

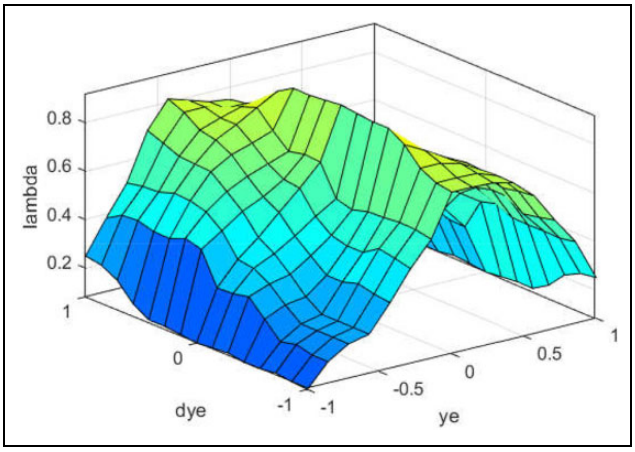

Figure 2. The fuzzy surface.

Velocity tracking control

u_d denotes the desired absolute surge velocity, as shown in Figure 3. To facilitate calculation, we generally choose the desired relative surge velocity as our control objective. The rationality is analyzed in Remark 2. For simplicity, we assume $u_r=\hat{u}_r$ in this section. Define $u_e=\hat{u}_r-u_{rd}$ and the sliding surface $s_1=u_e+c_1\int_0^t u_e d\tau$, where c_1 is a positive parameter to be designed. The derivative of s_1 is

$$\dot{s}_1=\underbrace{H_u(v_r,r)-\frac{d_{11}}{m_{11}}u_r}_{g_u}-\dot{u}_d+\tau_u+\delta_u+c_1u_e \tag{28}$$

Subsequently, by virtue of FLS to approximate the external model uncertainties $\hat{g}_u=\hat{\theta}_u\xi_a(s_1)$.

To solve the problem of input saturation, an auxiliary dynamic system is proposed as

$$\dot{\sigma}_u=\begin{cases}-k_{\sigma u}\sigma_u-\dfrac{|s_1\Delta\tau_u+0.5\kappa^2\Delta\tau_u^2|}{\sigma_u}+\kappa\Delta\tau_u, |\sigma_u|\geq\sigma_k \\ 0, |\sigma_u|<\sigma_k\end{cases} \tag{29}$$

where $k_{\sigma u}$, κ, and σ_k are positive constants, and $\Delta t_u=\tau_u-\tau_{u0}$. The corresponding nominal surge control law is proposed as

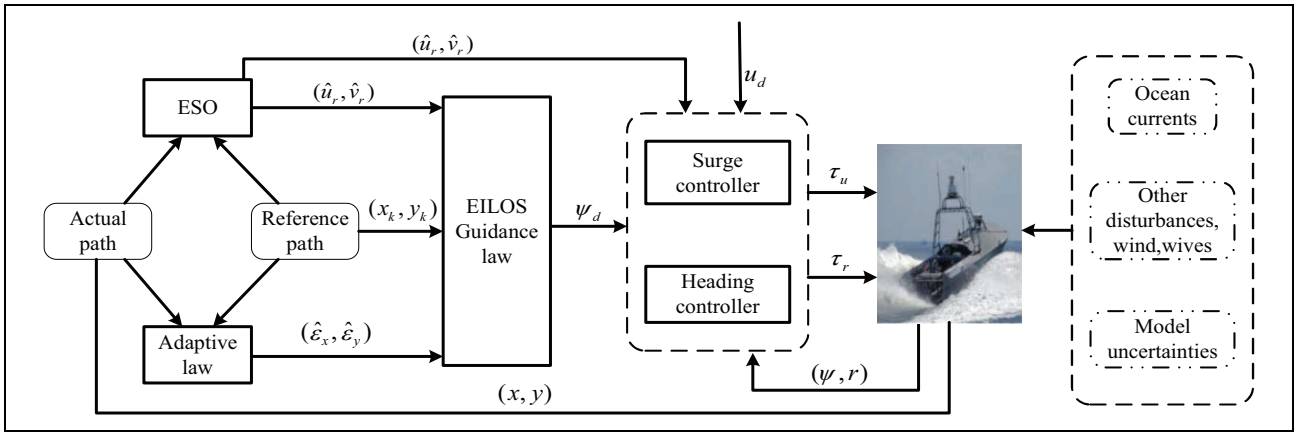

Figure 3. Block diagram of the proposed USV path following strategy. USV: unmanned surface vehicle.

$$\tau_{u0} = -\hat{\theta}_u \xi_a(s_1) + \dot{u}_d - \eta_1 sgn(s_1) - c_1 u_e - k_u s_1 + k_{u0}\sigma_u \tag{30}$$

where η_1 is the upper bound of δ_u and is unknown. In addition, the sign function $\mathrm{sgn}(s_1)$ will cause system input chattering. Therefore, we define that $\hat{h}_1 = \hat{\theta}_{h1}\xi_b(s_1)$ represents the approximation to $\eta_1 sgn(s_1)$. The control law can be rewritten as

$$\tau_{u0} = -\hat{\theta}_u \xi_a(s_1) + \dot{u}_d - \hat{h}_1 - c_1 u_e - k_u s_1 + k_{u0}\sigma_u \tag{31}$$

The update laws of FLS are proposed as follows

$$\begin{cases} \dot{\hat{\theta}}_u = \gamma_1 \left(s_1 \xi_a(s_1) - \rho_u \hat{\theta}_u \right) \\ \dot{\hat{\theta}}_{h1} = p_1 \left(s_1 \xi_b(s_1) - q_u \hat{\theta}_{h1} \right) \end{cases} \tag{32}$$

where γ_1, ρ_u, p_1 and q_u are positive parameters.

Theorem 2. All of the errors of the USV path-following velocity control system are UUB with the control law (31) and the update law (32).

Proof. Assign the following LFC $V_u = \frac{1}{2}s_1^2 + \frac{1}{2\gamma_1}\tilde{\theta}_u^T\tilde{\theta}_u + \frac{1}{2p_1}\tilde{\theta}_{h1}^T\tilde{\theta}_{h1} + \frac{1}{2}\sigma_u^2$, where $\tilde{\theta}_u = \theta_u - \hat{\theta}_u$ and $\tilde{\theta}_{h1} = \theta_{h1} - \hat{\theta}_{h1}$.

When $|\sigma_u| \geq \sigma_k$, the time derivative of V_u is

$$\begin{aligned} \dot{V}_u = \; & s_1 \left(\tilde{\theta}_u^T \xi_a(s_1) + \varepsilon_u - k_u s_1 - \hat{\theta}_{h1}^T \xi_b(s_1) + \theta_{h1}^T \xi_b(s_1) \right. \\ & \left. - \theta_{h1}^T \xi_b(s_1) + \delta_u + k_{u0}\sigma_u + \Delta\tau_u \right) + \sigma_u \left(-k_{\sigma u}\sigma_u \right. \\ & \left. - \frac{|s_1 \Delta\tau_u + 0.5\kappa^2 \Delta\tau_u^2|}{\sigma_u^2}\sigma_u + \kappa\Delta\tau_u \right) - \frac{1}{\gamma_1}\tilde{\theta}_u^T \dot{\hat{\theta}}_u \\ & - \frac{1}{p_1}\tilde{\theta}_{h1}^T \dot{\hat{\theta}}_{h1} \end{aligned} \tag{33}$$

In view of equation (32) and Lemma 3, we have

$$\begin{aligned} \dot{V}_u \leq \; & -\left(k_u - 1 - \frac{1}{2}k_{u0} \right) s_1^2 - \left(k_{\sigma u} - \frac{k_{u0}}{2} - \frac{1}{2} \right) \sigma_u^2 \\ & - \frac{\rho_u}{2}\tilde{\theta}_u^T\tilde{\theta}_u - \frac{q_u}{2}\tilde{\theta}_{h1}^T\tilde{\theta}_{h1} + s_1\delta_u - \eta_1|s_1| + \frac{1}{2}(\varepsilon_u^2 \\ & + \varepsilon_{h1}^2) + \frac{\rho_u}{2}\theta_{u\max}^T\theta_{u\max} + \frac{q_u}{2}\theta_{h1\max}^T\theta_{h1\max} \\ & \leq -2\mu_{u1}V_u + C_{u1} \end{aligned} \tag{34}$$

where ε_u and ε_{h1} are the approximation errors of g_u and $\mathrm{sgn}(s_1)$

$\mu_{u1} = \min\{k_u - 1 - \frac{1}{2}k_{u0}, k_{\sigma u} - \frac{k_{u0}}{2} - \frac{1}{2}, \frac{\rho_u\gamma_1}{2}, \frac{q_u p_1}{2}\}$ and $C_{u1} = \frac{1}{2}(\varepsilon_u^2 + \varepsilon_{h1}^2) + \frac{\rho_u}{2}\theta_{u\max}^T\theta_{u\max} + \frac{q_u}{2}\theta_{h1\max}^T\theta_{h1\max}$.

When $|\sigma_u| < \sigma_k$, we do not need to analyze the boundness of σ_u, so the LFC can become $V_u = \frac{1}{2}s_1^2 + \frac{1}{2\gamma_1}\tilde{\theta}_u^T\tilde{\theta}_u + \frac{1}{2p_1}\tilde{\theta}_{h1}^T\tilde{\theta}_{h1}$, and then, we have

$$\begin{aligned} \dot{V}_u \; & = s_1 \left(\tilde{\theta}_u^T \xi_a(s_1) + \varepsilon_u - k_u s_1 - \hat{\theta}_{h1}^T \xi_b(s_1) + \theta_{h1}^T \xi_b(s_1) \right. \\ & \quad \left. - \theta_{h1}^T \xi_b(s_1) + \delta_u + k_{u0}\sigma_u + \Delta\tau_u \right) \\ & \quad - \frac{1}{\gamma_1}\tilde{\theta}_u^T \gamma_1 \left(s_1 \xi(s_1) - \rho_u \hat{\theta}_u \right) \\ & \quad - \frac{1}{p_1}\tilde{\theta}_{h1}^T p_1 \left(s_1 \xi(s_1) - q_u \hat{\theta}_{h1} \right) \\ & \leq -\left(k_u - \frac{3}{2} - \frac{1}{2}k_{u0} \right) s_1^2 - \frac{\rho_u}{2}\tilde{\theta}_u^T\tilde{\theta}_u - \frac{q_u}{2}\tilde{\theta}_{h1}^T\tilde{\theta}_{h1} \\ & \quad + \frac{1}{2}\left(\varepsilon_u^2 + \varepsilon_{h1}^2 \right) + \frac{\rho_u}{2}\theta_{u\max}^T\theta_{u\max} + \frac{1}{2}k_{u0}\sigma_u^2 \\ & \quad + s_1\delta_u - \eta_1|s_1| + \frac{1}{2}\Delta\tau_u^2 + \frac{q_u}{2}\theta_{h1\max}^T\theta_{h1\max} \\ & \leq -2\mu_{u2}V_u + C_{u2} \end{aligned} \tag{35}$$

where $\mu_{u2} = \min\{k_u - \frac{3}{2} - \frac{1}{2}k_{u0}, \frac{\rho_u\gamma_1}{2}, \frac{q_u p_1}{2}\}$ and $C_{u2} = \frac{1}{2}\left(\varepsilon_u^2 + \varepsilon_{h1}^2\right) + \frac{\rho_u}{2}\theta_{u\max}^T\theta_{u\max} + \frac{q_u}{2}\theta_{h1\max}^T\theta_{h1\max} + \frac{1}{2}\Delta\tau_u^2 + \frac{1}{2}k_{u0}\sigma_u^2$.

Synthesizing equations (34) and (35), we have

$$\dot{V}_u \le -2\mu_u V_u + C_u \tag{36}$$

where $\mu_u = \min\{\mu_{u1}, \mu_{u2}\}$ and $C_u = \max\{C_{u1}, C_{u2}\}$. Thus, V_u is a monotone decreasing function out of the range $\varpi_2 = \{V_u \le \frac{C_u}{2\mu_u}\}$ and that gives

$$V_u \le (V_u(0) - \frac{C_u}{2\mu_u})e^{-2\mu_u t} + \frac{C_u}{2\mu_u} \tag{37}$$

It follows that all of the error signals of the velocity tracking subsystem are UUB from Lemma 1, and the subsystem is stable. Without the assumption $u_r = \hat{u}_r$, the stability of the velocity tracking system can also be guaranteed (see the literature[65]).

Attitude tracking control

Define attitude tracking error $\psi_e = \psi - \psi_d$ and the sliding surface $s_2 = c_2\psi_e + \dot{\psi}_e$, where c_2 is a positive constant. Differentiating both sides of s_2 with respect to time results in

$$\dot{s}_2 = c_2\dot{\psi}_e - \ddot{\psi}_d + \underbrace{H_r(u_r, v_r, r)}_{g_r} + \tau_r + \delta_r \tag{38}$$

Similar to the last subsection, the auxiliary system is given by

$$\dot{\sigma}_r = \begin{cases} -k_{\sigma r}\sigma_r - \dfrac{|s_2\Delta\tau_u + 0.5\kappa^2\Delta\tau_r^2|}{\sigma_r} + \kappa\Delta\tau_r, |\sigma_r| \ge \sigma_k \\ 0, |\sigma_r| \le \sigma_k \end{cases} \tag{39}$$

where $\Delta t_r = \tau_r - \tau_{r0}$ and $k_{\sigma r}$ is a positive parameter. In view of the unascertained bound of δ_r, the nominal heading control law τ_{r0} is designed as

$$\tau_{r0} = -\hat{\theta}_r\xi_a(s_2) - c_2\dot{\psi}_e + \ddot{\psi}_d - \hat{h}_2 - k_r s_2 - \psi_e + k_{r0}\sigma_r \tag{40}$$

where $\hat{g}_r = \hat{\theta}_r\xi_a(s_2)$ represents the approximation of g_r and $\hat{h}_2 = \hat{\theta}_{h2}\xi_b(s_2)$. The update laws are presented as

$$\begin{cases} \dot{\hat{\theta}}_r = \gamma_2\left(s_2\xi_a(s_2) - \rho_r\hat{\theta}_r\right) \\ \dot{\hat{\theta}}_{h2} = p_2\left(s_2\xi_b(s_2) - q_r\hat{\theta}_{h2}\right) \end{cases} \tag{41}$$

where γ_2, ρ_r, p_2, and q_r are positive parameters.

Theorem 3. All of the tracking errors of the USV attitude control system are UUB with the control law (40) and the update law (41).

Proof. Considering the following LFC $V_r = \frac{1}{2}\psi_e^2 + \frac{1}{2}s_2^2 + \frac{1}{2\gamma_2}\tilde{\theta}_r^T\tilde{\theta}_r + \frac{1}{2p_2}\tilde{\theta}_{h2}^T\tilde{\theta}_{h2} + \frac{1}{2}\sigma_r^2$.

When $|\sigma_r| \ge \sigma_k$, the derivative of V_r yields

$$\begin{aligned} \dot{V}_r = & -c\psi_e^2 + \psi_e s_2 + s_2\Big(\tilde{\theta}_r^T\xi_a(s_2) + \varepsilon_r - k_r s - \psi_e + \Delta\tau_r \\ & + \hat{\theta}_{h2}^T\xi_b(s_2) + \theta_{h2}^T\xi_b(s_2) - \theta_{h2}^T\xi_b(s_2) + \delta_r + k_{r0}\sigma_r\Big) \\ & + \sigma_r\left(-k_{\sigma r}\sigma_r - \frac{|s_2\Delta\tau_r + 0.5\kappa^2\Delta\tau_r^2|}{\sigma_r^2}\sigma_r + \kappa\Delta\tau_r\right) \\ & - \frac{1}{\gamma_2}\tilde{\theta}_r^T\dot{\hat{\theta}}_r - \frac{1}{p_2}\tilde{\theta}_{h2}^T\dot{\hat{\theta}}_{h2} \end{aligned} \tag{42}$$

Substituting equation (41) into (42) and using Lemma 3 yields

$$\begin{aligned} \dot{V}_r \le & -\left(k_r - 1 - \frac{1}{2}k_{r0}\right)s_2^2 - \left(k_{\sigma r} - \frac{k_{r0}}{2} - \frac{1}{2}\right)\sigma_r^2 \\ & - c\psi_e^2 - \frac{\rho_r}{2}\tilde{\theta}_r^T\tilde{\theta}_r - \frac{q_r}{2}\tilde{\theta}_{h2}^T\tilde{\theta}_{h2} + \frac{1}{2}\left(\varepsilon_r^2 + \varepsilon_{h2}^2\right) \\ & + \frac{\rho_r}{2}\theta_{r\max}^T\theta_{r\max} + \frac{q_r}{2}\theta_{h2\max}^T\theta_{h2\max} + s_2\delta_r - \eta_3|s_2| \\ & \le -2\mu_{r1}V_r + C_{r1} \end{aligned} \tag{43}$$

where $\mu_{r1} = \min\{c, k_r - 1 - \frac{1}{2}k_{r0}, k_{\sigma r} - \frac{k_{r0}}{2} - \frac{1}{2}, \frac{\rho_r}{2}, \frac{q_r}{2}\}$ and $C_{r1} = \frac{1}{2}\left(\varepsilon_r^2 + \varepsilon_{h2}^2\right) + \frac{\rho_r}{2}\theta_{r\max}^T\theta_{r\max} + \frac{q_r}{2}\theta_{h2\max}^T\theta_{h2\max}$.

When $|\sigma_r| < \sigma_k$, similar to V_u, V_r can become $V_r = \frac{1}{2}\psi_e^2 + \frac{1}{2}s_2^2 + \frac{1}{2\gamma_2}\tilde{\theta}_r^T\tilde{\theta}_r + \frac{1}{2p_2}\tilde{\theta}_{h2}^T\tilde{\theta}_{h2}$, and differentiating V_r gives

$$\begin{aligned} \dot{V}_r = & c_2\psi_e^2 + \psi_e s_2 + s_2\Big(\tilde{\theta}_r^T\xi_a(s_2) + \varepsilon_r - k_r s - \psi_e + \Delta\tau_r \\ & + \hat{\theta}_{h2}^T\xi_b(s_2) + \theta_{h2}^T\xi_b(s_2) - \theta_{h2}^T\xi_b(s_2) + \delta_r + k_{r0}\sigma_r\Big) \\ & - \frac{1}{\gamma_2}\tilde{\theta}_r^T\dot{\hat{\theta}}_r - \frac{1}{p_2}\tilde{\theta}_{h2}^T\dot{\hat{\theta}}_{h2} \\ & \le -c_2\psi_e^2 - \left(k_r - \frac{3}{2} - \frac{1}{2}k_{r0}\right)s_2^2 - \frac{\rho_r}{2}\tilde{\theta}_r^T\tilde{\theta}_r \\ & - \frac{q_r}{2}\tilde{\theta}_{h2}^T\tilde{\theta}_{h2} + \frac{1}{2}\Delta\tau_r^2 + \frac{1}{2}k_{r0}\sigma_r^2 + \frac{1}{2}\left(\varepsilon_r^2 + \varepsilon_{h2}^2\right) \\ & + \frac{\rho_r}{2}\theta_{r\max}^T\theta_{r\max} + \frac{q_r}{2}\theta_{h2\max}^T\theta_{h2\max} + s_2\delta_r \\ & - \eta_3|s_2| \\ & \le -2\mu_{r2}V_r + C_{r2} \end{aligned} \tag{44}$$

where $\mu_{r2} = \min\{c_2, k_r - 1 - \frac{1}{2}k_{r0}, \frac{\rho_r}{2}, \frac{q_r}{2}\}$ and $C_r = \frac{1}{2}\Delta\tau_r^2 + \frac{1}{2}k_{r0}\sigma_r^2 + \frac{1}{2}\left(\varepsilon_r^2 + \varepsilon_{h2}^2\right) + \frac{\rho_r}{2}\theta_{r\max}^T\theta_{r\max} + \frac{q_r}{2}\theta_{h2\max}^T\theta_{h2\max}$. From the above, we could reach

$$\dot{V}_r \le -2\mu_r V_r + C_r \tag{45}$$

where $\mu_r = \min\{\mu_{r1}, \mu_{r2}\}$ and $C_r = \max\{C_{r1}, C_{r2}\}$. Thus, V_r is a monotone decreasing function out of the range $\varpi_3 = \{V_r \leq \frac{C_r}{2\mu_r}\}$, and then, we have

$$V_r \leq \left(V_r(0) - \frac{C_r}{2\mu_r}\right)e^{-2\mu_r t} + \frac{C_r}{2\mu_r} \tag{46}$$

We can conclude that all of the error signals of the attitude tracking subsystem are UUB from Lemma 1, and the subsystem is stable.

Closed-loop system stability analysis

Theorem 4. Define the tracking errors $\zeta_e = [\boldsymbol{X}_e, \boldsymbol{Y}_e, \boldsymbol{Z}_e]^{\mathrm{T}}$, where $\boldsymbol{X}_e = [x_e, y_e]^{\mathrm{T}}$, $\boldsymbol{Y}_e = [s_1, \psi_e, s_2]^{\mathrm{T}}$, and $\boldsymbol{Z}_e = [\tilde{u}_r, \tilde{v}_r, \tilde{\theta}_x, \tilde{\theta}_y, \tilde{\theta}_u, \tilde{\theta}_r, \tilde{\theta}_{h1}, \tilde{\theta}_{h2}]^{\mathrm{T}}$, in the presence of model uncertainties, ocean currents, and other unknown disturbances. If the mathematical model of USV is defined as equation (5), the guidance law is calculated by equation (15), the controllers are designed by equations (31) and (40), based on Assumptions 1 to 5, we have the following conclusions:

1. All of the tracking errors and estimation errors of the closed-loop system are UUB, and the system is stable.
2. The sway velocity is passively bounded.

Proof. For the closed-loop system of USV.

1. Assign the complete LFC $V = V_1 + V_u + V_r$. The derivative of V with respect to time satisfies $\dot{V} \leq \mu_1 V_1 + \mu_u V_u + \mu_r V_r + C_1 + C_u + C_r \leq \mu V + C$, where $\mu = \min\{\mu_1, \mu_u, \mu_r\}$ and $C = C_1 + C_u + C_r$ such that

$$V \leq (V(0) - \frac{C}{2\mu})e^{-2\mu t} + \frac{C}{2\mu} \tag{47}$$

It follows that all the errors of the closed-loop system are UUB, thus, the USV path following system is stable. It is indicated that ζ_e ultimately converges to the range $\{\zeta_e \in \mathbb{R}^5, ||\zeta_e|| \leq \frac{C}{\mu}\}$. We can see from equation (50) that the ultimate compact set can be adjusted by tuning control parameters $k_1, k_2, k_u, k_r, k_{u0}, k_{r0}$, and so on.

2. For the sway velocity v_r, consider a Lyapunov function $V_v = \frac{1}{2}v_r^2$, differentiating it with respect to time, we have

$$\begin{aligned} \dot{V}_v &= \boldsymbol{F}(u_r)v_r^2 + \boldsymbol{E}(u_r)rv_r + \delta_v v_r \\ &\leq \boldsymbol{F}(u_r)v_r^2 + |\boldsymbol{E}(u_r)r + \delta_v||v_r| \end{aligned} \tag{48}$$

where $\boldsymbol{F}(u_r) < 0$ and $\boldsymbol{E}(u_r)r + \delta_v$ are bounded.[19] Therefore, v_r is bounded referring to Chapter 4.8 of the literature.[66]

Table 2. Control parameters of USV simulation.

Notation	Value	Notation	Value	Notation	Value
k_1	1.5	κ	1	p_1	5
k_2	3	σ_k	0.001	p_2	5
Γ_1	1	k_{u0}	4	q_u	0.1
Γ_2	1	k_{r0}	2	q_r	0.2
ϑ_1	0.1	γ_1	10	c_1	1
ϑ_2	0.05	γ_2	30	c_2	1
$k_{\sigma u}$	1.5	ρ_u	0.2	k_u	1
$k_{\sigma r}$	2.5	ρ_r	0.3	k_r	2

USV: unmanned surface vehicle.

Simulation studies

To illustrate the availability of the proposed path following scheme, some simulation studies are conducted in this section with USV, whose parameters can be found in the literature.[19] The look-ahead distance is defined as $\Delta_{\min} = 6, \Delta_{\max} = 12$. The absolute value of (τ_u, τ_r) is restricted to (2 N, 1.5 Nm).[67] The control parameters are given in Table 2. The time-varying ocean currents within the inertial frame are set as $V_x = 0.03\sin(t/20)$ m/s and $V_y = 0.02\sin(t/20)$ m/s. The other disturbances are assumed to be $[\delta_u, \delta_v, \delta_r]^{\mathrm{T}} = [0.15\sin(0.1t), 0.1\sin(0.1t), 0.15\sin(0.1t)]^{\mathrm{T}}$. To emphasize the superiority of the method proposed in this article, we take the PLOS[12] and CLOS[18] methods as position comparisons and the ELOS method as USV velocity estimation comparisons, where ELOS represents the proposed EILOS scheme without dealing with the ocean currents. Note that the ocean currents were not taken into account in the literature,[12] therefore, we consider the same ocean currents as in the EILOS scheme and employ the same adaptive strategy to treat them. Specifically, we consider the USV's relative resultant velocities as measurable states in the PLOS and CLOS schemes because they calculate the sideslip angles instead of USV velocities. In addition, the backstepping method is contrasted for ψ_e and u_{e1} in the control part, where $u_{e1} = u_{rd} - u_r$.

The velocity u_{rd} is set to 0.6 m/s, and the initial USV states are given by $[x(0), y(0), u_r(0), v_r(0), r(0), \psi(0)] = [0, 15, 0.5, 0.01, 0, 0]$. The initial values of $\hat{u}_r$ and $\hat{v}_r$ are (0.3, 0.15). The reference path is

$$\begin{cases} x_k(\varsigma) = 30\sin(0.1\varsigma) + \varsigma \\ y_k = 3\varsigma \end{cases} \tag{49}$$

Results are depicted in Figures 4 to 14. Figures 4 and 5 show that the USV can follow the reference path, and the proposed EILOS scheme performs best because it converges to the reference path in minimal time. In addition, the PLOS and CLOS schemes exhibit obvious fluctuations in cross-tracking error, y_e, at the steady period. Figure 7 indicates that the unmeasured surge and sway velocities can be precisely and quickly extracted using the proposed

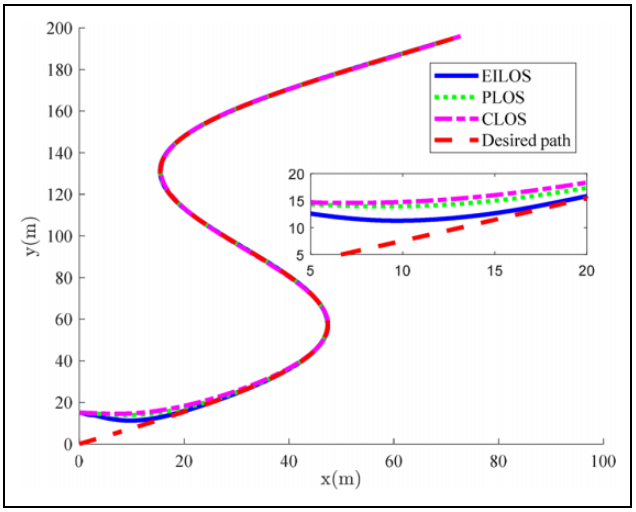

Figure 4. Path following performance.

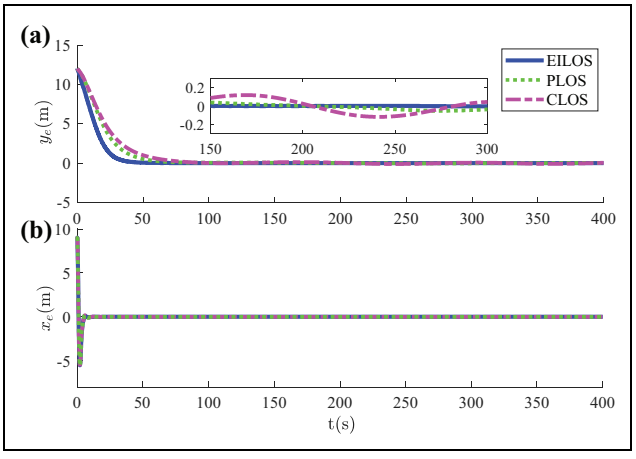

Figure 5. (a) Cross- and (b) along-track errors.

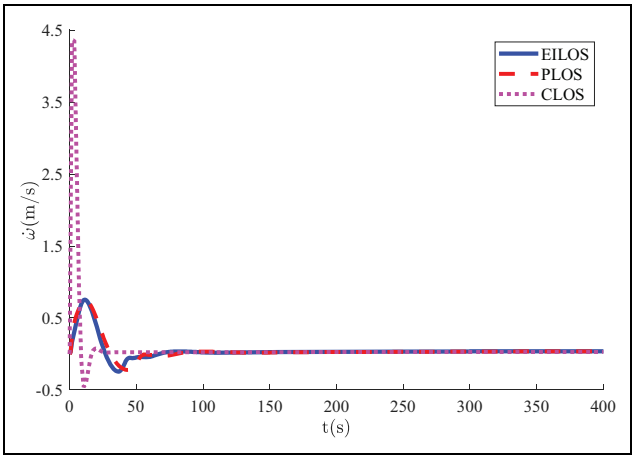

Figure 6. The update law of path variable.

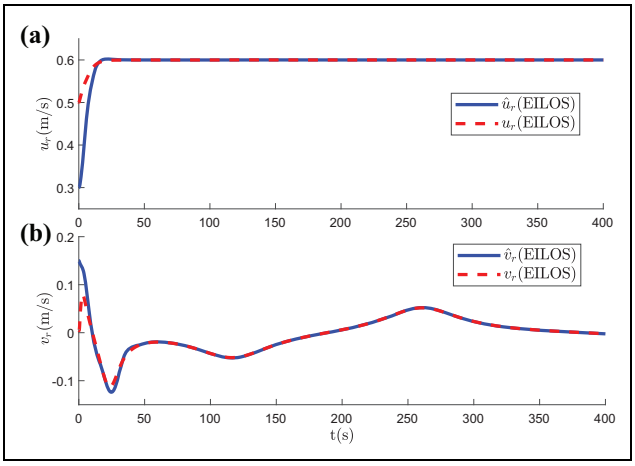

Figure 7. (a) The velocities and (b) their estimations.

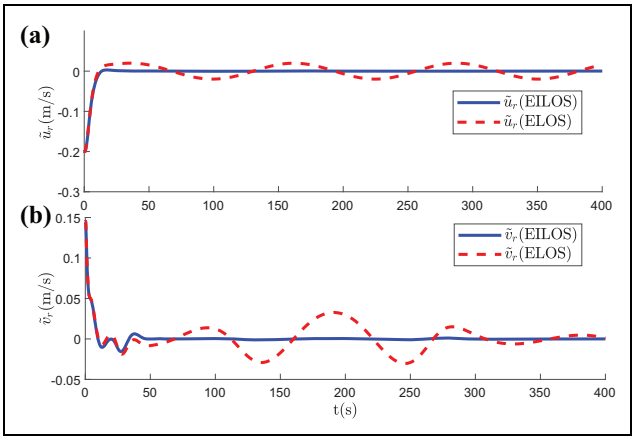

Figure 8. (a, b) The estimate errors of USV velocities. USV: unmanned surface vehicle.

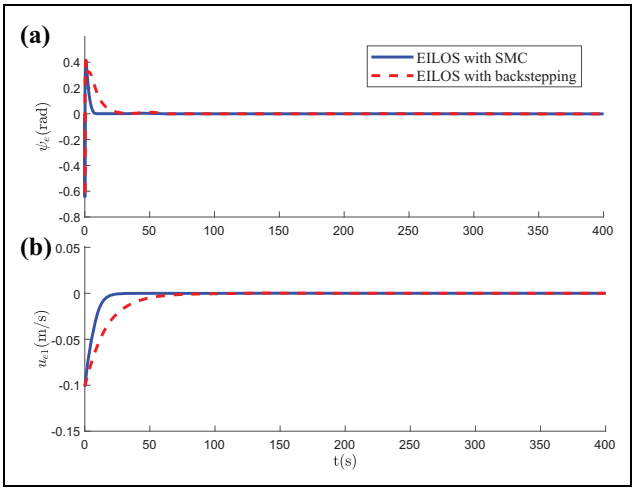

Figure 9. (a, b) The attitude and surge velocity tracking errors.

ESO. Furthermore, it is reasonable to compare the relative USV resultant velocities as measurable states in the PLOS and CLOS schemes. If ocean currents are not compensated in the ELOS scheme, as shown in Figure 8, then obvious fluctuations exist in the velocity estimate errors. Attitude and surge velocity tracking errors are displayed in Figure 9,

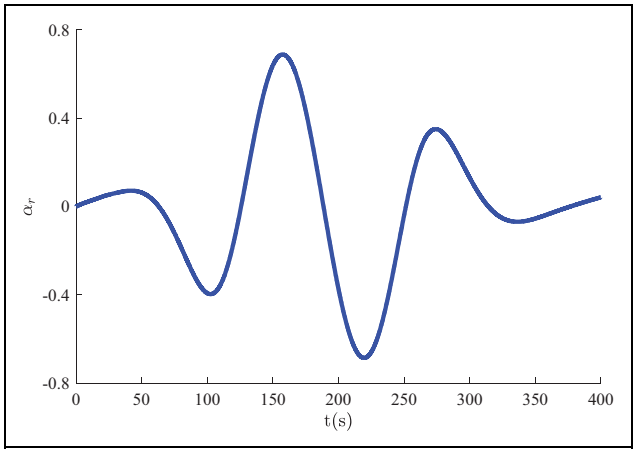

Figure 10. The performance of α_r.

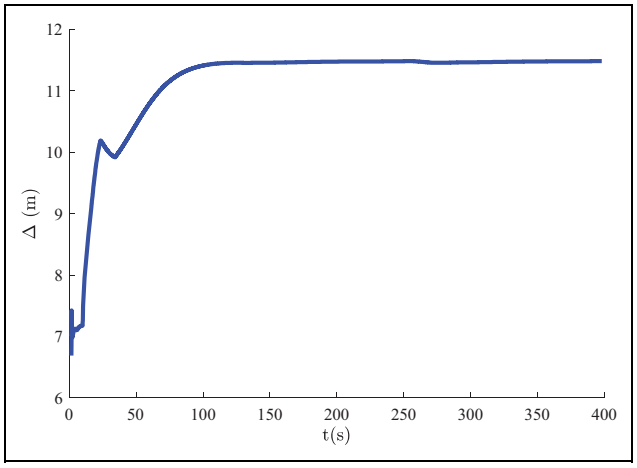

Figure 11. Look-ahead distance.

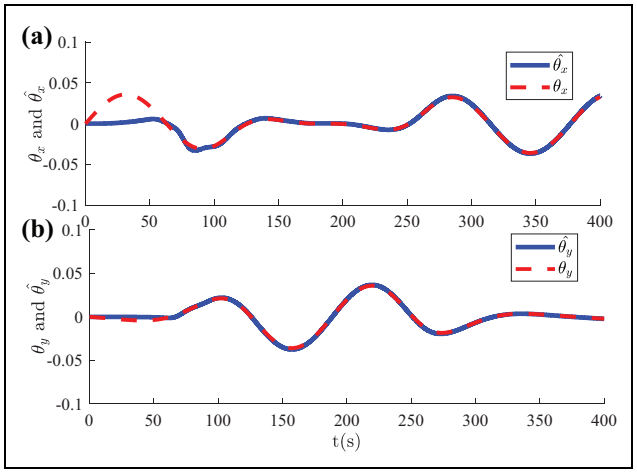

Figure 12. (a, b) Ocean current parameters and their estimations.

in which the SMC and backstepping methods can each cause (ψ, u_r) to converge to (ψ_d, u_{rd}), and the SMC method exhibits a faster response. Figure 10 illustrates that the virtual control input α_r canceling the drift term is bound,

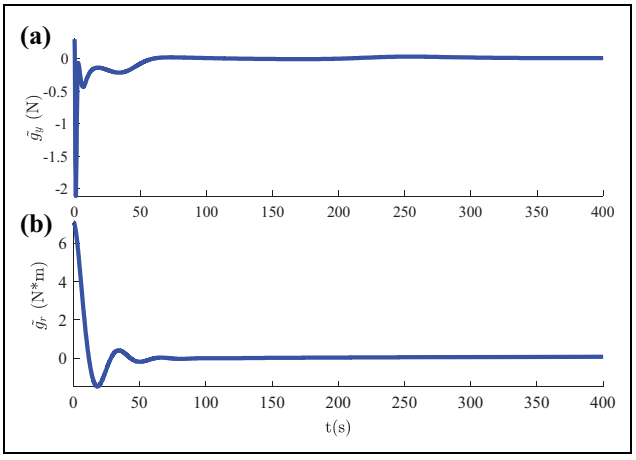

Figure 13. (a, b) The approximation errors of unknown dynamics.

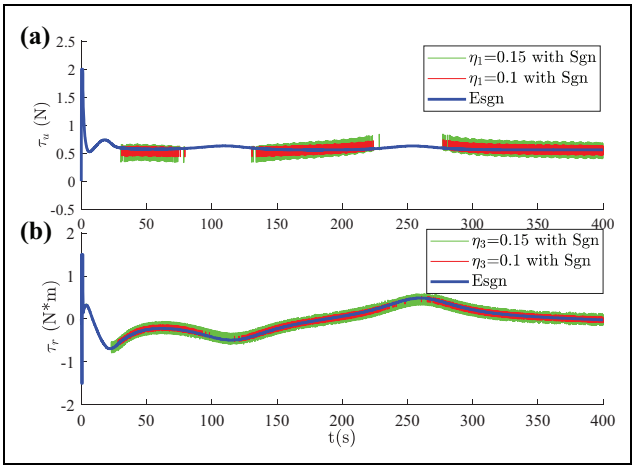

Figure 14. (a, b) The control inputs.

and the bound is small. Figure 11 shows the value of Δ, as the aforementioned theory, Δ increases as y_e decreases. Ocean current parameters and their estimates appear in Figure 12, in which the estimates $(\hat{\theta}_x, \hat{\theta}_y)$ can be identified by the adaptive method. Figure 13 describes the approximation errors of model uncertainties (i.e. g_u and g_r), and the FLS has an excellent approximation effect. Last, the performance of input signals is shown in Figure 14, revealing that the control inputs are within the allowable range once auxiliary dynamic systems are added. In addition, a comparison analysis between the control input with sign functions and with the estimations of sign functions (esgn) by FLS is also depicted in Figure 14, in which we can see that the problem of chattering is solved by FLS and control inputs satisfy engineering applications.

Conclusions

In this article, an ISMC is proposed based on a novel ESO, an ILOS guidance law, an auxiliary dynamic system, and the FLS. The salient features of the proposed algorithm

are as follows. First, the unmeasured velocity can be precisely estimated by ESO. Second, the ILOS guidance law is able to provide the reference heading angle as well as estimating the ocean current velocities simultaneously. Third, the ISMC with FLS is able to force the state tracking errors converge to a neighborhood of zero. It is verified that the closed-loop system of the USV is UUB. The simulation results show the availability and superiority of the EIAFSM scheme.

Many problems warrant closer investigation, and some methods must be enhanced for USV path following (e.g. neglecting the hysteresis characteristic of the actuator and the lack of an accurate adaptive method for fast time-varying ocean currents). Therefore, disturbance observers are powerful tools that will be the focus of our subsequent work.

Declaration of conflicting interests

The author(s) declared no potential conflicts of interest with respect to the research, authorship, and/or publication of this article.

Funding

The author(s) disclosed receipt of the following financial support for the research, authorship, and/or publication of this article: This work was supported by "the National Natural Science Foundation of China" [Grant numbers 51879027, 51579024, and 51809028] and "the Fundamental Research Funds for the Central Universities" [Grant numbers 3132019318 and 3132019109].

ORCID iD

Mingcong Li https://orcid.org/0000-0002-5687-8870

References

1. Fossen TI, Pettersen KY, and Galeazzi R. Line-of-sight path following for Dubins paths with adaptive sideslip compensation of drift forces. *IEEE Trans Control Syst Technol* 2015; 23(2): 820–827.
2. Zhang J, Yu S, and Yan Y. Fixed-time extended state observer-based trajectory tracking and point stabilization control for marine surface vessels with uncertainties and disturbances. *Ocean Eng* 2019; 186(15): 106109.
3. Shojaei K. Neural adaptive robust control of underactuated marine surface vehicles with input saturation. *Appl Ocean Res* 2015; 53: 267–278.
4. Sun T, Zhang J, and Pan Y. Active disturbance rejection control of surface vessels using composite error updated extended state observer. *Asian J Control* 2017; 19(5): 1802–1811.
5. Miao B and Li T. A novel neural network-based adaptive control for a class of uncertain nonlinear systems in strict feedback form. *Nonlin Dynam* 2015; 79(2): 1005–1013.
6. He B, Wang S, and Liu Y. Underactuated robotics: a review. *Int J Adv Rob Syst* 2019;16(4): 1–29.
7. He B, Cao X, and Gu Z. Kinematics of underactuated robotics for product carbon footprint. *J Clean Prod* 2020; 257: 120491.
8. He B, Liu Y, Zeng L, et al. Product carbon footprint across sustainable supply chain. *J Clean Prod* 2019; 241: 118320.
9. Zhang A, Lai X, Wu M, et al. Nonlinear stabilizing control for a class of underactuated mechanical systems with multi degree of freedoms. *Nonlin Dynam* 2017; 89: 2241–2253.
10. Chen Y and Tian Y. Formation tracking and attitude synchronization control of underactuated ships along closed orbits. *Int J Robust Nonlin* 2015; 25: 3023–3044.
11. Healey A and Lienard D. Multivariable sliding mode control for autonomous diving and steering of unmanned underwater vehicles. *IEEE J Ocean Eng* 1993; 18(3): 327–339.
12. Liu L, Wang D, Peng Z, et al. Predictor-based los guidance law for path following of underactuated marine surface vehicles with sideslip compensation. *Ocean Eng* 2016; 124: 340–348.
13. Kelasidi E, Liljeback P, Pettersen KY, et al. Integral line-of-sight guidance for path following control of underwater snake robots: theory and experiments. *IEEE Trans Rob* 2017; 33(3): 1–19.
14. Bevly DM, Sheridan R, and Pettersen KY. Integrating INS sensors with GPS velocity measurements for continuous estimation of vehicle sideslip and tire cornering stiffness. In: *American automatic control conference, AACC*, Washington, USA, 25–27 June 2001, pp. 483–493.
15. Mu D, Wang G, Fan Y, et al. Adaptive LOS path following for a podded propulsion unmanned surface vehicle with uncertainty of model and actuator saturation. *Appl Sci* 2017; 7(12): 1232–1251.
16. Liu L, Wang D, and Peng Z. ESO-based line-of-sight guidance law for path following of underactuated marine surface vehicles with exact sideslip compensation. *IEEE J Ocean Eng* 2017; 42(2): 477–487.
17. Wang N, Sun Z, Yin J, et al. Finite-time observer based guidance and control of underactuated surface vehicles with unknown sideslip angles and disturbances. *IEEE Access* 2018; 6: 14059–14070.
18. Miao J, Wang S, Tomovic M, et al. Compound line-of-sight nonlinear path following control of underactuated marine vehicles exposed to wind, waves, and ocean currents. *Nonlin Dynam* 2017; 89(4): 2441–2459.
19. Zheng Z and Sun L. Path following control for marine surface vessel with uncertainties and input saturation. *Neurocomputing* 2016; 177(C): 158–167.
20. Sussmann HJ. A general theorem on local controllability. *SIAM J Control Optim* 1987; 25(1): 158–194.
21. Bianchini RM and Stefani G. Controllability along a trajectory: a variational approach. *SIAM J Control Optim* 1993; 31(4): 900–927.
22. Hermann R and Krener A. Nonlinear controllability and observability. *IEEE Trans Autom Control* 1977; 22(5): 728–740.
23. Arai H, Tanie K, and Tachi S. Dynamic control of a manipulator with passive joints in operational space. *IEEE Trans Robot Autom* 1993; 9: 85–93.

24. Nakamura Y, Suzuki T, and Koinuma M. Nonlinear behavior and control of a nonholonomic free-joint manipulator. *IEEE Trans Robot Autom* 1997; 13: 853–862.
25. Levine WS.Open-loop control using oscillatory inputs. In: *The control systems handbook*. Boca Raton: Chemical Rubber Company Press, 2010, pp. 1191–1211.
26. Yu Y, Guo C, and Yu H. Finite-time predictor line-of-sight based adaptive neural network path following for unmanned surface vessels with unknown dynamics and input saturation. *Int J Adv Rob Syst* 2018; 15(6): 172988141881469.
27. Do KD, Jiang ZP, and Pan J. Robust adaptive path following of underactuated ships. *Automatica* 2004; 40(6): 929–944.
28. Wang R, Wang S, Wang Y, et al. Path following for a biomimetic underwater vehicle based on ADRC. In: *IEEE international conference on robotics and automation, ICRA*, Singapore, 29 May–3 June 2017, pp. 3519–3524. IEEE.
29. Liu Y, Zhu J, Li R, et al. Omni-directional mobile robot controller based on trajectory linearization. *Rob Autom Syst* 2008; 56(5): 461–479.
30. Ashrafiuon H, Muske KR, McNinch LC, et al. Sliding mode tracking control of surface vessels. *IEEE Trans Ind Electron* 2008; 55(11): 4004–4012.
31. Ouyang P, Acob J, and Pano V. PD with sliding mode control for trajectory tracking of robotic system. *Rob Comput Integr Manuf* 2014; 30(2): 189–200.
32. Matveev A, Wang C, and Savkin A. Real-time navigation of mobile robots in problems of border patrolling and avoiding collisions with moving and deforming obstacles. *Rob Autom Syst* 2012; 60(6): 769–788.
33. Bessa W, Dutra M, and Kreuzer E. Depth control of remotely operated underwater vehicles using an adaptive fuzzy sliding mode controller. *Rob Autom Syst* 2008; 56(8): 670–677.
34. Veysi M, Soltanpour M, and Khooban M. A novel self-adaptive modified bat fuzzy sliding mode control of robot manipulator in presence of uncertainties in task space. *Robotica* 2015; 33(10): 2045–2064.
35. Chen Y, Yan Y, Wang K, et al. An adaptive fuzzy sliding mode controller for the depth control of an underactuated underwater vehicle. *Int J Adv Rob Syst* 2019; 16(2): 1–10.
36. Nikkhah M, Ashrafiuon H, and Fahimi F. Robust control of underactuated bipeds using sliding modes. *Robotica* 2007; 25: 367–374.
37. Ashrafiuon H and Erwin RS. Shape change maneuvers for attitude control of underactuated satellites. In: *Proceedings of the 2005 american control conference*, Portland, OR, USA, 8–10 June 2005, pp. 895–900. IEEE.
38. Almutairi NB and Zribi M. Sliding mode control of a three-dimensional overhead crane. *J Vib Control* 2009; 15: 1679–1730.
39. Van M, Kang H J, Suh Y S, et al. Output feedback tracking control of uncertain robot manipulators via higher-order sliding-mode observer and fuzzy compensator. *J Mech Sci Technol* 2013; 27(8): 2487–2496.
40. Liang X, Wan L, Blake J, et al. Path following of an underactuated AUV based on fuzzy backstepping sliding mode control. *Int J Adv Rob Syst* 2016; 13(3): 1.
41. Meng Q, Zhang T, Gao X, et al. Adaptive sliding mode fault-tolerant control of the uncertain Stewart platform based on offline multibody dynamics. *IEEE ASME Trans Mechatron* 2014; 19(3): 882–894.
42. Yu H, Guo C, and Yan Z. Globally finite-time stable three-dimensional trajectory-tracking control of underactuated UUVs. *Ocean Eng* 2019; 189: 106329.
43. Jin M, Jin Y, Hun P, et al. High-accuracy tracking control of robot manipulators using time delay estimation and terminal sliding mode. *Int J Adv Rob Syst* 2011; 8(4): 65–78.
44. Jia H, Zhang L, Cheng X, et al. Three-dimensional path following control for an underactuated UUV based on nonlinear iterative sliding mode. *Zidonghua Xuebao Acta Auto Sin* 2012; 38(2): 308–314.
45. Cheng C, Liu S, and Wu H. A transformed Lure problem for sliding mode control and chattering reduction. *IEEE Trans Autom Control* 1999; 44(3): 563–568.
46. Su W, Drakunov S, Ozguner U., et al. Sliding mode with chattering reduction in sampled data systems. In: *IEEE conference on decision and control*, San Antonio, TX, USA, 15–17 December 1993, pp. 2452–2457. Piscataway, NJ, United States: IEEE.
47. Yoo B and Ham W. Adaptive fuzzy sliding mode control of nonlinear system. *IEEE Trans Fuzzy Syst* 1998; 6(2): 315–321.
48. Konno Y and Hashimoto H. Design of sliding mode dynamics in the frequency domain. *Adv Rob* 1992; 7(6): 587–598.
49. Khorashadizadeh S and Fateh MM. Uncertainty estimation in robust tracking control of robot manipulators using the Fourier series expansion. *Robotica* 2017; 35(2): 310–336.
50. Coelho P and Nunes U. Path-following control of mobile robots in presence of uncertainties. *IEEE Trans Rob* 2005; 21(2): 252–261.
51. Liu H and Zhang T. Neural network-based robust finite-time control for robotic manipulators considering actuator dynamics. *Rob Comput Integr Manuf* 2013; 29(2): 301–308.
52. Xiang X, Yu C, and Zhang Q. Robust fuzzy 3D path following for autonomous underwater vehicle subject to uncertainties. *Comput Oper Res* 2017; 84: 165–177.
53. Tao Y, Zheng J, and Lin Y. A sliding mode control-based on a RBF neural network for deburring industry robotic systems. *Int J Adv Rob Syst* 2016; 13(1): 1.
54. Wang N, Sun Z, Zheng Z, et al. Finite-time sideslip observer-based adaptive fuzzy path-following control of underactuated marine vehicles with time-varying large sideslip. *Int J Fuzzy Syst* 2018; 20(6): 1767–1778.
55. Wang N and Er MJ. Self-constructing adaptive robust fuzzy neural tracking control of surface vehicles with uncertainties and unknown disturbances. *IEEE Trans Control Syst Technol* 2015; 23(3): 991–1002.
56. Chen M, Ge SS, and Ren B. Adaptive tracking control of uncertain MIMO nonlinear systems with input constraints. *Automatica* 2011; 47(3): 452–465.
57. Su Y and Swevers J. Finite-time tracking control for robot manipulators with actuator saturation. *Rob Comput Integr Manuf* 2014; 30(2): 91–98.

58. Loria A and Panteley E. Cascaded nonlinear time-varying systems: analysis and design. *Lect Notes Control Inf Sci* 2005; 311: 23–64.
59. Ge SS and Wang C. Adaptive neural control of uncertain MIMO nonlinear systems. *IEEE Trans Neural Netw* 2004; 15(3): 674–692.
60. Hardy GH, Littlewood JE, and Polya G. *Inequalities. Reprint' of the 1952 edition*. Cambridge: Cambridge Mathematical Library, 1988.
61. Lekkas AM and Fossen TI. Integral LOS path following for curved paths based on a monotone cubic hermite spline parametrization. *IEEE Trans Control Syst Technol* 2014; 22(6): 2287–2301.
62. Fossen TI. *Handbook of marine craft hydrodynamics and motion control*. Trondheim: John Wiley & Sons, 2011.
63. Caoyang Y, Chunhu L, Lian L, et al. ELOS-based path following control for underactuated surface vehicles with actuator dynamics. *Ocean Eng* 2019; 187(1): 106139.
64. Fossen TI and Lekkas AM. Direct and indirect adaptive integral line-of-sight path-following controllers for marine craft exposed to ocean currents. *Int J Adapt Control Signal Process* 2017; 31(4): 445–463.
65. Wang Y, Tong H, and Wang C. High-gain observer-based line-of-sight guidance for adaptive neural path following control of underactuated marine surface vessels. *IEEE Access* 2019; 7: 26088–26101.
66. Khalil HK. Boundedness and ultimate boundedness. In: Khalil HK (ed) *Nonlinear systems*. 3rd ed. New Jersey: Prentice Hall, 2002, pp. 168–174.
67. Fredriksen E and Pettersen KY. Global-exponential waypoint maneuvering of ships: theory and experiments. *Automatica* 2006; 42(4): 677–687.

Appendix

$$\boldsymbol{H}_u(v_r, r) = \frac{(m_{22}r + m_{23}r)r}{m_{11}}$$

$$\boldsymbol{H}_r(u_r, v_r, r) = \frac{m_{23}d_{22} - m_{22}(d_{32} + (m_{22} - m_{11})u_r)}{m_{22}m_{33} - m_{23}^2}v_r + \frac{m_{23}(d_{23} + m_{11}u_r) - m_{22}(d_{33} + m_{23}u_r)}{m_{22}m_{33} - m_{23}^2}r$$

$$\boldsymbol{E}(u_r) = \frac{m_{23}^2 - m_{11}m_{33}}{m_{22}m_{33} - m_{23}^2}u_r + \frac{d_{33}m_{23} - d_{23}m_{33}}{m_{22}m_{33} - m_{23}^2}$$

$$\boldsymbol{F}(u_r) = \frac{(m_{22} - m_{11})m_{23}}{m_{22}m_{33} - m_{23}^2}u_r - \frac{d_{22}m_{33} - d_{32}m_{23}}{m_{22}m_{33} - m_{23}^2}$$